Improving embrittlement in the Ti-Al-C MAX phase system: a composite approach for surface severe plastic deformation

Adrien Heinzelmeier, Antoine Guitton, Marc Novelli, Wenbo Yu, Thierry Grosdidier

Improving embrittlement in the Ti-Al-C MAX phase system: A composite approach for surface severe plastic deformation

Adrien Heinzelmeier [a], Antoine Guitton [a,b,*], Marc Novelli [a,b], Wenbo Yu [c], Thierry Grosdidier [a,b,*]

[a] Université de Lorraine, CNRS, Arts et Métiers, LEM3, Metz, France
[b] Laboratory of Excellence on Design of Alloy Metals for low-mAss Structures (DAMAS), Université de Lorraine, Metz, France
[c] Center of Materials Science and Engineering, School of Mechanical and Electronic Control Engineering, Beijing Jiaotong University, Beijing, China

ARTICLE INFO

Article history:
Received 29 September 2022
Received in revised form 7 March 2023
Accepted 1 April 2023
Available online 3 April 2023

Keywords:
MAX phases
Severe plastic deformation (SPD)
Surface modification

ABSTRACT

Ti_2AlC and Ti_3AlC_2 belong to an interesting family of layered compounds called MAX phases. A composite approach is tested here to improve the intrinsic brittle behaviour of such compounds. To this end, a bulk MAX compound and a MAX/$TiAl_2$ composite have been deformed under surface severe plastic deformation (SSPD) by surface mechanical attrition treatment (SMAT). Grain delamination and grain decohesion occurred to a depth of 100 µm below the surface for the bulk compound. Resulting cracks and grain pullouts were witnessed by a decrease in the surface and sub-surface hardness. Comparatively, the presence of intergranular $TiAl_2$ effectively prevented such failure for the composite. Thus, the SSPD of this cohesive composite created a surface hardening (+60%) gradient extending down to a depth of 250 µm. Witness marks of plasticity were revealed in both the MAX and $TiAl_2$ phases.

1. Introduction

$M_{n+1}AX_n$ phases (where n = 1–3) are composed of a transition metal M, an A-group element A and usually nitrogen and/or carbon for X [1]. MAX phases belong to a promising class of materials because of their potentially wide range of applications. They combine properties of both ceramics (refractory, high stiffness, low density at room temperature) and metals (high thermal and electric conductivity, thermal shock resistance, mechanical resistance). MAX phases have a layered structure with a hexagonal lattice (space group: $P6_3/mmc$) and they exhibit an elevated crystalline anisotropy ($c/a > 3$) [2]. It is commonly observed that during their synthesis, grains of MAX phases grow as platelet in a stack of atomic layers parallel to basal planes [3]. These platelets have a high aspect ratio, because of the high crystalline anisotropy. The platelet grain shape is likely to foster grain decohesion from stress concentrations at grain boundaries [4,5]. It is established that MAX phases deform by kink bands (KB) [2]. Under further deformation, KBs lead to buckling and formation of delamination cracks within individual grains [6]. Moreover, due to their particular crystallography and their particular grain shape, these materials involve mainly strong plastic anisotropy, non-Schmid effects and lack of independent glide systems [4,5,7,8]. MAX phases exhibit a brittle-to-ductile transition around 800 °C thus leading to massive failure after a very limited plastic regime at room temperature and pressure [1,9,10].

Regardless of the material, surfaces in particular are exposed to complex solicitations during service (wear, higher stress concentration, corrosion.), so that they are often the site for fracture initiations. Therefore, one of the major concerns for engineers is to explore original routes allowing surface tailoring. Promising intense shot peening techniques, such as ultrasonic shot peening (USP) or surface mechanical attrition treatment (SMAT) involving surface severe plastic deformation (SSPD), have been used to modify the surface and improve properties [11–18]. In particular, the SMAT technique proceeds via numerous collisions of the peening media having random trajectories inside a confined chamber [11,12,14,15].

As one could expect on a brittle material, no SSPD has been tested to date on MAX phases. However, unlike most ceramics, an individual MAX phase grain is quite damage tolerant [7,19]. Failure occurs through grain decohesion, because of the weak binding force at grain boundaries. In an attempt to prevent it, a composite approach is used here to strengthen the MAX phase grain boundaries. This study reports the first results of SSPD on MAX phases and the

relevance of the composite approach to achieve a resistant gradient material.

2. Materials and methods

2.1. Material processing

A fully dense Ti_2AlC material was synthesized by powder metallurgy as detailed in [20]. Briefly, 99.5 wt% purity powders of Ti, Al and TiC were mixed in stoichiometric proportions and pressure less sintered at 1400 °C. This first material will be referred to as *bulk material* throughout the article. A second material was sintered in contact with oxygen at 1400 °C and subsequent cooling leading to a mixture of MAX phases with an additional intergranular phase. This second material will be referred to as *composite material* throughout the article.

2.2. Initial microstructures

X-ray diffraction (XRD) was carried out using a cobalt X-ray tube on both the *bulk* and *composite* materials. The different phases were further analysed by Scanning Electron Microscopy (SEM) using a Zeiss Supra 40 FEG-SEM (Oberkochen, Germany) coupled with Energy-dispersive X-ray spectroscopy (EDS). The relative fractions of the different phases were estimated by image analysis of several SEM micrographs using the FIJI software. Grain sizes were estimated by mean linear intercept method in random directions using the FIJI software.

Fig. 1 plots the diffractograms acquired by XRD. The *bulk material* is mainly composed of Ti_2AlC. Some Al_2O_3 and possibly some traces of Ti_3AlC_2 within uncertainty of XRD are also revealed by the analysis of the XRD peaks. In comparison, the XRD diffractogram of the *composite material* revealed essentially Ti_3AlC_2, with additional $TiAl_2$ and traces of Al_2O_3. The identified structure for $TiAl_2$ is the $L1_0$ based superstructure of $HfGa_2$-type [21].

Typical micrographs imaged under backscattered electrons (BSE) conditions are given in Fig. 2 together with EDS maps. The overall quantification results are gathered in Table 1 together with hardness values.

Both in the *bulk material* (Fig. 2.a.) and the *composite material* (Fig. 2.b.), Ti-Al-C MAX phases appear in the brightest contrast. Al_2O_3 appears in the darkest contrast while $TiAl_2$ appears in dark grey contrast around the Ti_3AlC_2 grains of the *composite material* (Fig. 2.b.). This is better seen at higher magnification in Fig. 2.c. The *bulk material* is composed of 99.4% Ti_2AlC and 0.6% Al_2O_3, while the *composite* is composed of 89.4 vol% Ti_3AlC_2, 2.5% Al_2O_3 and about 8% $TiAl_2$ (Table 1).

Titanium, aluminium, carbon and oxygen EDS mappings made in the same region are given in Fig. 2.d. They confirm the expected distributions of different elements in the identified phases. Each phase composition provided in Table 1 was determined by EDS point quantification as the mean value of five measurements. The compositions agree well with the different stoichiometry of the phases.

The formation of Ti_xAl_y intermetallics between MAX phase grains has already been documented after synthesis [7,22]. Our EDS quantifications and the Ti-Al phase diagram [23] have confirmed the intermetallic to be $TiAl_2$. Under oxidation, the Ti_2AlC decomposes into TiC by forming an intermediate phase of Ti_3AlC_2 while Al diffuses easily along the MAX phase basal planes to form the Al_2O_3 oxide [20]. Consistently, the MAX phase composition after oxidation is closer to Ti_3AlC_2 than Ti_2AlC within the *composite material*. Due to the different processing conditions, the average size of the Ti_3AlC_2 grains (19 µm) is slightly larger than the Ti_2AlC one (15 µm).

2.3. Deformation and characterisation of the deformed states

SMAT was carried out for 3 min using 100C6 Ø2 mm spherical shots set in motion by a sonotrode vibrating at 20 kHz with an amplitude of 40 µm using a Sonats *stressonic* equipments (Carquefou, France). Vickers microhardness were measured using a Zwick Roell microindenter (Ulm, Germany). The in-depth evolution of hardness after SMAT was conducted using a 100 g load for a step size of 50 µm. Each hardness value is an average of six indentation results with an error bar representing one standard deviation (± σ). Grain internal misorientations were mapped with the electron backscatter diffraction (EBSD) technique and analysed with the ATEX software developed at LEM3 laboratory (Metz, France) [26]. For better imaging conditions, the samples where ionically polished in a Gatan PECS II (Pleasanton, USA). The crystallographic defects within the different phases were further observed in the SEM by Electron Channelling Contrast Imaging (ECCI) [27–31].

3. Results

3.1. Microstructures after SMAT

Fig. 3 compares BSE micrographs of the *bulk* and *composite materials* cross-sections after SMAT, with deformed surfaces facing top.

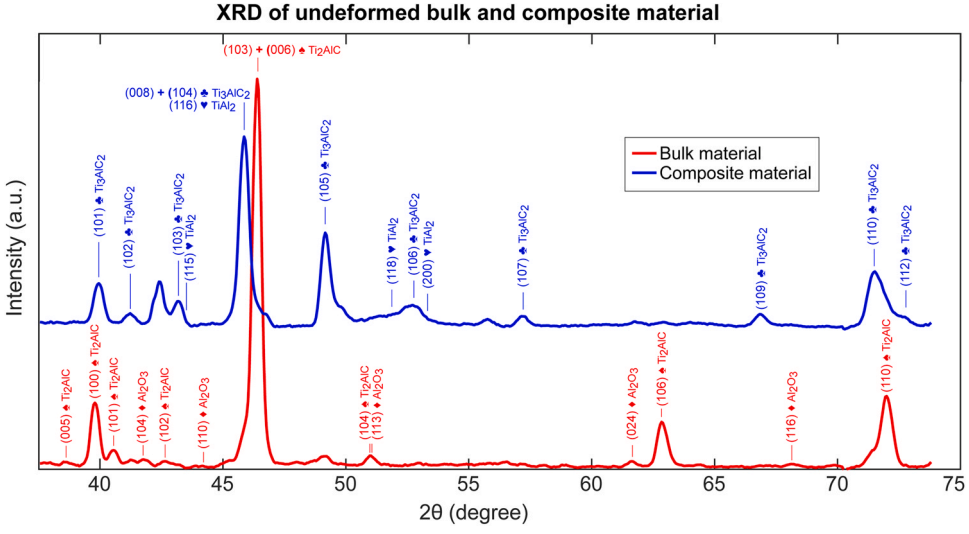

Fig. 1. XRD diffractograms of both *bulk* and *composite* materials before SMAT.

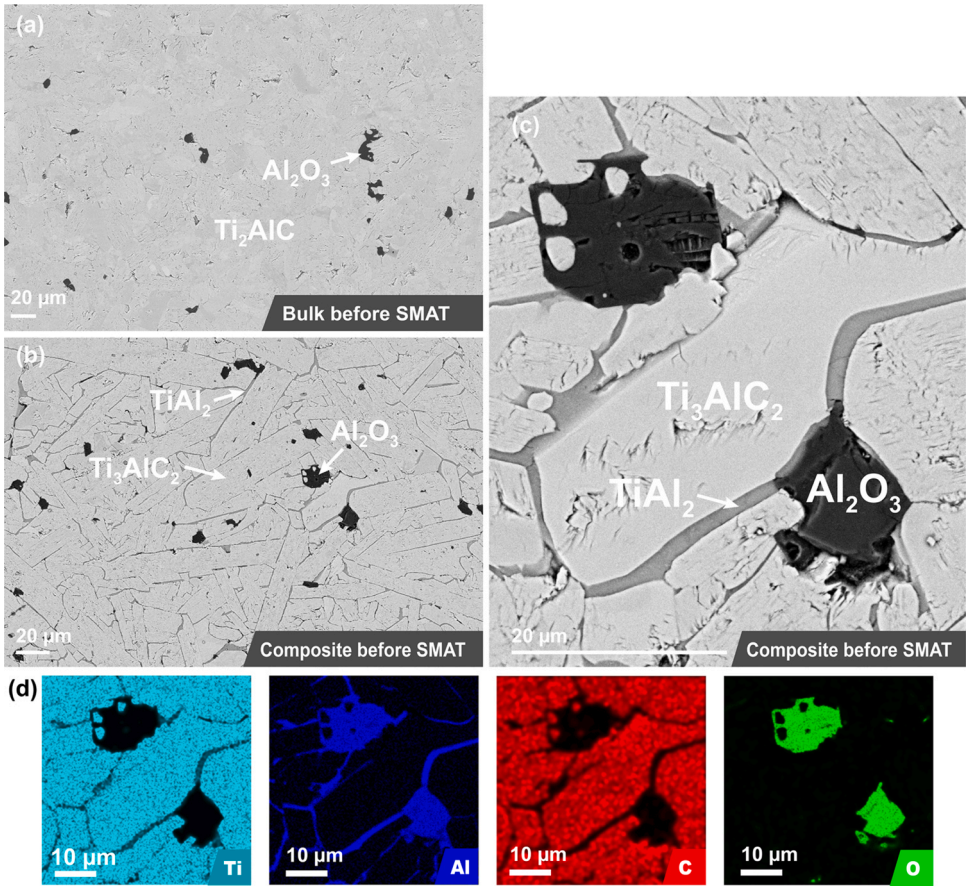

Fig. 2. BSE micrographs of (a) *bulk* and (b) *composite*. (c) Higher magnification BSE micrograph of the composite (d) and its corresponding Ti, Al, C, O EDS maps.

Table 1
Characterisation of the as-sintered materials.

	EDS quantification [at%]				µ-hardness	Image analysis phase fraction (%)		
	Ti	Al	C	O	HV0.1	MAX phases	$TiAl_2$	Al_2O_3
Bulk material	47.9	20.1	23.8	8.2	337	99.4	-	0.6
Composite material	43.2	18.1	26.6	12.0	409	89.4	8.1	2.5
Ti_2AlC [at%]	52.8	22.7	24.5	-	337			
Ti_3AlC_2 [at%]	53.1	16.2	30.7	-	357[24]			
$TiAl_2$ [at%]	34.5	65.5	-	-	600[25]			
Al_2O_3 [at%]	-	39.6	-	60.4	-			

First, it appears that the surface of the *bulk material* is damaged (Fig. 3.a.), as opposed to the *composite material* which has retained its surface integrity (Fig. 3.b.). Second, a layer of severely cracked grains damaged by SMAT can be measured to a depth of 100 µm inside the *bulk material* (Fig. 3.c.). The higher magnification micrograph in Fig. 3.e. better shows the important number of cracks within and between the Ti_2AlC grains. Intragranular cracks are either arrowed as "delamination" or "perpendicular cracks", respectively aligned with or perpendicular to the MAX phase platelets. Local grain decohesion and pullout are arrowed as well in Fig. 3.e. Comparatively, less damage occurred in the *composite material*, as only slight delamination and almost no grain decohesion nor pullout are visible in Fig. 3.f.

3.2. Microhardness gradients

Fig. 4 plots the Vickers microhardness evolutions measured on the cross-section at different depths from the deformed surfaces. As shown in the insets, indentations cover multiple grains, thus providing a mean hardness value of the different phase mixtures composing the materials.

Whereas the hardness of the *bulk material* drops near the treated surface, the composite material is effectively hardened, reaching 648 HV (+58%) at a depth of 50 µm. Towards the material cores, both curves reach a plateau consistent with the hardness measured before SMAT, respectively 409 HV for the *composite* and 337 HV for the *bulk* (Table 1).

As previously stated, the structure of the MAX phase is different in the *bulk* and *composite* samples, as it changed from Ti_2AlC to Ti_3AlC_2 due to the oxidation process. Since the mechanical properties of Ti_2AlC and Ti_3AlC_2 are very close [2] and both exhibit the same brittle behaviour, the MAX phase structure alone cannot explain the opposite evolution of the hardness gradients.

As the MAX phases are intrinsically hard and brittle, analysis of the defects in the different phases has been done in the following section to see if the strain hardening in the *composite* comes from the deformation of the binding intermetallic phase solely or if some hardening could also come from the MAX phases.

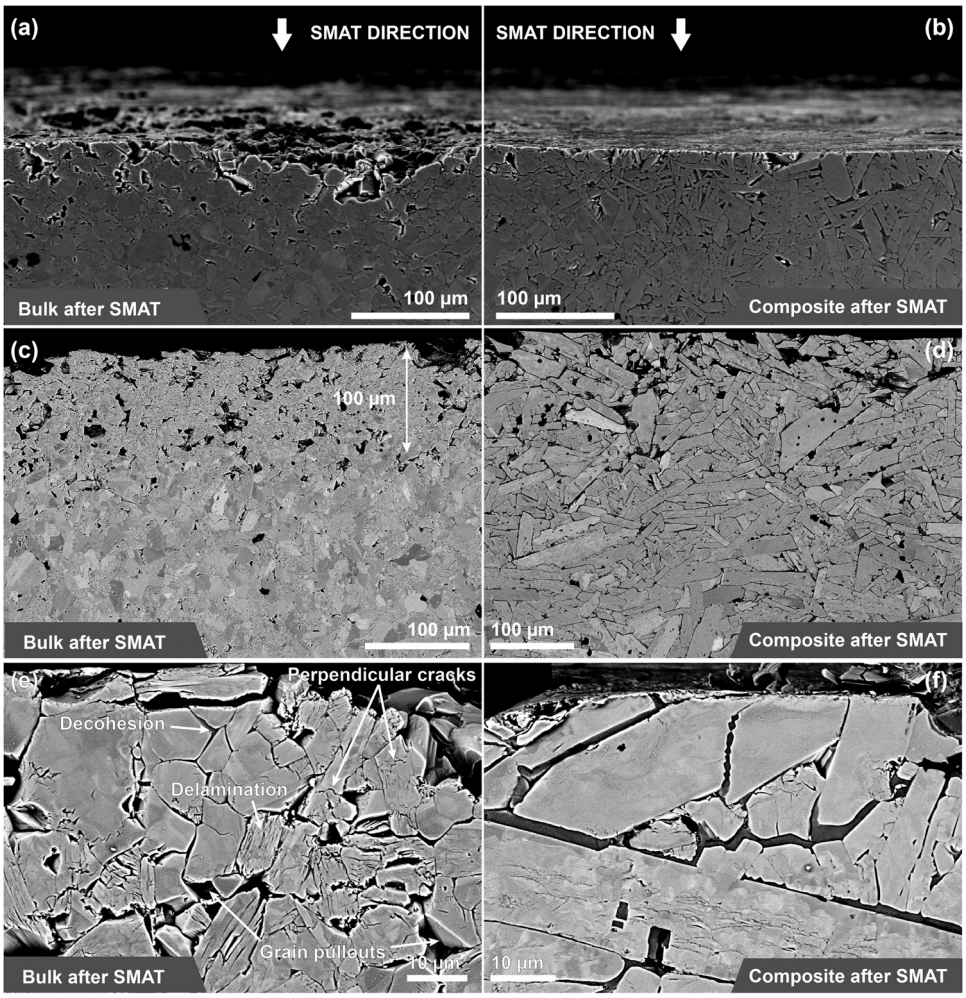

Fig. 3. BSE micrographs of *bulk material* (a,c,e) and *composite material* (b,d,f.) after SMAT. (a,b) surface aspect; (c,d) cross section of the surface and subsurface showing the affected zone; (e,f) higher magnification images showing structural defects at the treated surface.

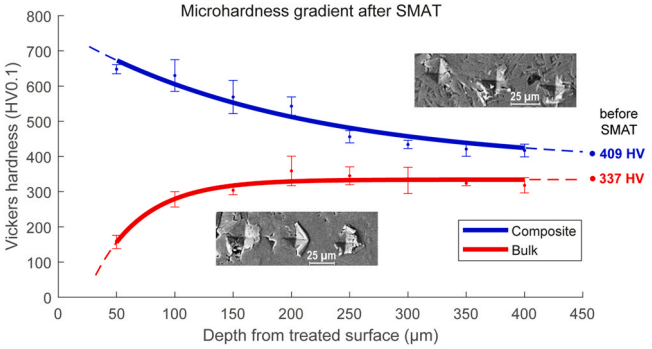

Fig. 4. Vickers microhardness gradients measured from the surfaces treated by SMAT. The insets show SEM micrographs of indentations left in the *composite* and *bulk* materials.

3.3. Lattice misorientations and crystallographic defects within the phases

Local lattice misorientations were calculated from the EBSD maps of both deformed materials. Fig. 5 represents the lattice misorientation angle relatively to the grain average orientation for each pixel in the MAX phases. Only misorientations above 3° are considered. For both materials after SMAT, the lattice misorientation in the MAX phases is of low magnitude, hardly exceeding 15°. The map of the *bulk material* in Fig. 5.a. shows higher lattice misorientation than the map of the *composite material* in Fig. 5.b. The bar graph in Fig. 5.c. better compares both material lattice misorientation by counting the number of pixels for each 0.5° angle of misorientation from 3° to 20°. This number of pixels is expressed as an area fraction of the micrograph. As shown in the bar graph the misoriented area is more than twice as big in the *bulk material* than in the *composite material*, for each misorientation value from 3° to 20°.

Fig. 6 gathers several micrographs of the *composite material* after SMAT for which the sample was slightly tilted (4.2°) under ECCI conditions – as explained in [30] – to visualize the structural defects within both the Ti_3AlC_2 MAX and $TiAl_2$ intermetallic phases. The MAX phase grain in the middle of Fig. 6.a. is located at 130 µm below the surface treated by SMAT. According to EBSD, the basal plane of this grain has only a 7.8° angle to the image plane of the micrograph. The edges of light grey contrast visible at the sample surface, marked by white arrows in Fig. 6.a., are due to the ionic polishing. These edges are visible in secondary electron imaging and cannot be mistaken with structural defects such as dislocations or sub-grain boundaries. A line of bright contrast consisting of dislocation pile-ups runs across the Ti_3AlC_2 grain. A higher magnification of a part of this pile-up is given in Fig. 6.b. Other dislocation networks are also visible within the MAX phase along the MAX/ $TiAl_2$ phase boundary imaged in Fig. 6.c. Such dislocation networks have already been observed in a MAX phase deformed at room temperature under confining pressure [32] and confirm the relative plasticity of the

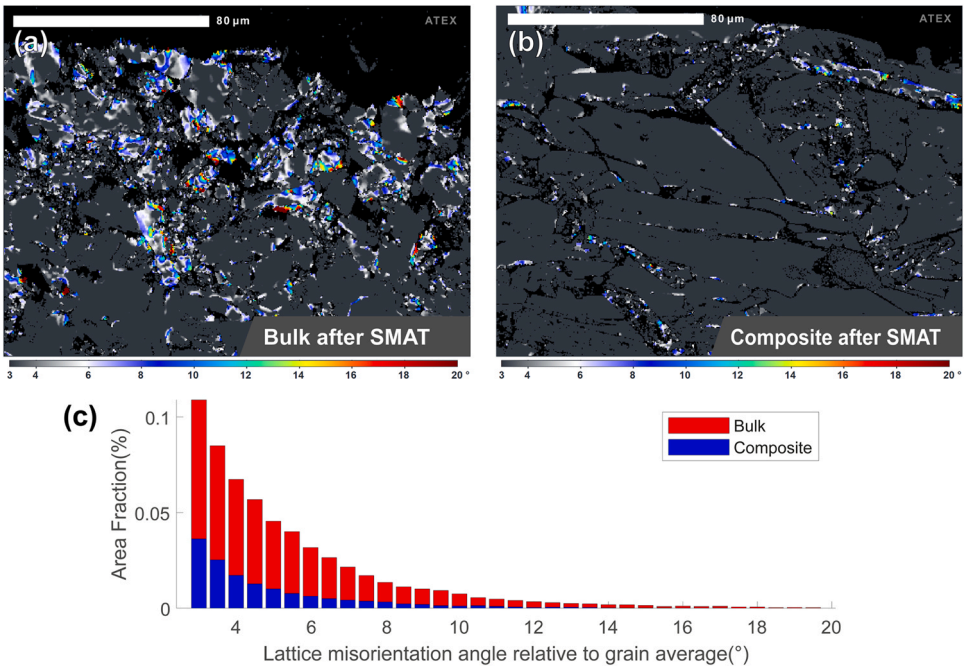

Fig. 5. Lattice misorientation relative to grain average orientation, drawn in ATEX software from EBSD maps. (a) shows the deformed *bulk*, (b) shows the deformed *composite*. (c) plots a wider area fraction of misorientations within the *bulk*.

MAX phase in response to the SMAT treatment. Several parallel straight-lined defects are visible within the $TiAl_2$ phase. They are better seen at higher magnification in Fig. 6.d. and 6.e. These straight lines suggest twins or antiphase boundaries (APB) within $TiAl_2$. They are a footprint of the intermetallic phase deformation and demonstrate its contribution to the hardening of the *composite material*. Further analysis on the exact nature of these structural defects is beyond the scope of the present contribution but should be done in a near future for a clear understanding of the deformation mechanisms in the $TiAl_2$ phase.

4. Discussion

A first interesting aspect revealed in the present contribution is the opposite response of the two materials to the same treatment. As shown in Fig. 4, while the hardness value drops towards the surface of the *bulk material*, the hardness increases up to 60% towards the surface of the *composite material*. Moreover, while the *composite material* has retained its surface integrity, the surface of the *bulk material* was damaged and the decohesion of several MAX phase grains was revealed. Since the mechanical properties of Ti_2AlC and Ti_3AlC_2 – respectively composing the majority of the *bulk* and *composite materials* – are very close [2] and both exhibit the same brittle behaviour, the MAX phase structure alone cannot explain the opposite evolution of the hardness gradients. These differences in behaviour can be understood by considering the deformation and damaging mechanisms of the MAX phases and the role of the binding intermetallic $TiAl_2$ phase present within the *composite material*.

For the *bulk material*, hardness starts to drop within 100 µm from the surface, which is the depth to where decohesion and delamination are visible in Fig. 3.c. As stated in the introduction part, MAX phases are brittle at room temperature and pressure. The most likely mechanism of failure is grain decohesion and/or delamination [2], respectively caused by intergranular and intragranular fracture [33]. In Fig. 3.e., two types of intragranular cracks are actually distinguishable: (i) those parallel to the platelet length, i.e. along basal planes due to delamination, and (ii) those perpendicular to the platelet length, due to the microstructure anisotropy of MAX phases as explained in [4,5]. These mechanisms were fully operative for the *bulk material*, thereby introducing damages to the first 100 µm under the surface during the SMAT operation. Grain decohesion is responsible for grain pullout at the sample surface and at the polished cross-section. Grain decohesion and delamination weaken the material, which hardness value drops below the phase intrinsic hardness [22]. It explains the drop in hardness of the *bulk material* despite the strain hardening of the MAX phase grains. In addition, because of the decohesion between the MAX phase grains near the surface, there is no load transfer towards the depth of the sample, so that no hardening is observed below the damaged zone of 100 µm in the *bulk material*.

For the *composite material,* the occurrence of decohesion/delamination events is drastically reduced despite it having a slightly coarser mean grain size. Although initially harder than its *bulk* counterpart, the *composite material* is much more cohesive under SMAT. This is due to the presence of the intergranular $TiAl_2$ intermetallic phase which is binding the Ti_3AlC_2 MAX phase in the *composite material*. Other literature studies have also reported that under uniaxial compression tests, the ductile Ti_xAl_y phases inhibit crack propagation within MAX phases [7]. Thus, the brittle behaviour of the MAX phases is successfully prevented by the presence of $TiAl_2$ for the *composite material*. The cohesive and preserved grains within the *composite material* are able to transfer the load imparted by the SMAT shots deeper in the microstructure. As seen in Fig. 6, deformation was witnessed both in the $TiAl_2$ phase and Ti_3AlC_2 MAX phase present in the *composite material*, resulting in a progressive hardening gradient reaching a depth of nearly 250 µm.

Even if surface hardening occurred under SMAT in our *composite material*, there are two important differences in the behaviour of this material compared to what is usually observed on processing of metals and alloys by SSPD. First, the hardening of the *composite material* is not due to surface nanocrystallisation by grain refinement. Actually, none of our *bulk* and *composite materials* have gone through any significative grain size reduction in the micrograph observations in Fig. 3. This is unlike metals usually hardened by SMAT, for which the surface hardening results from the formation of

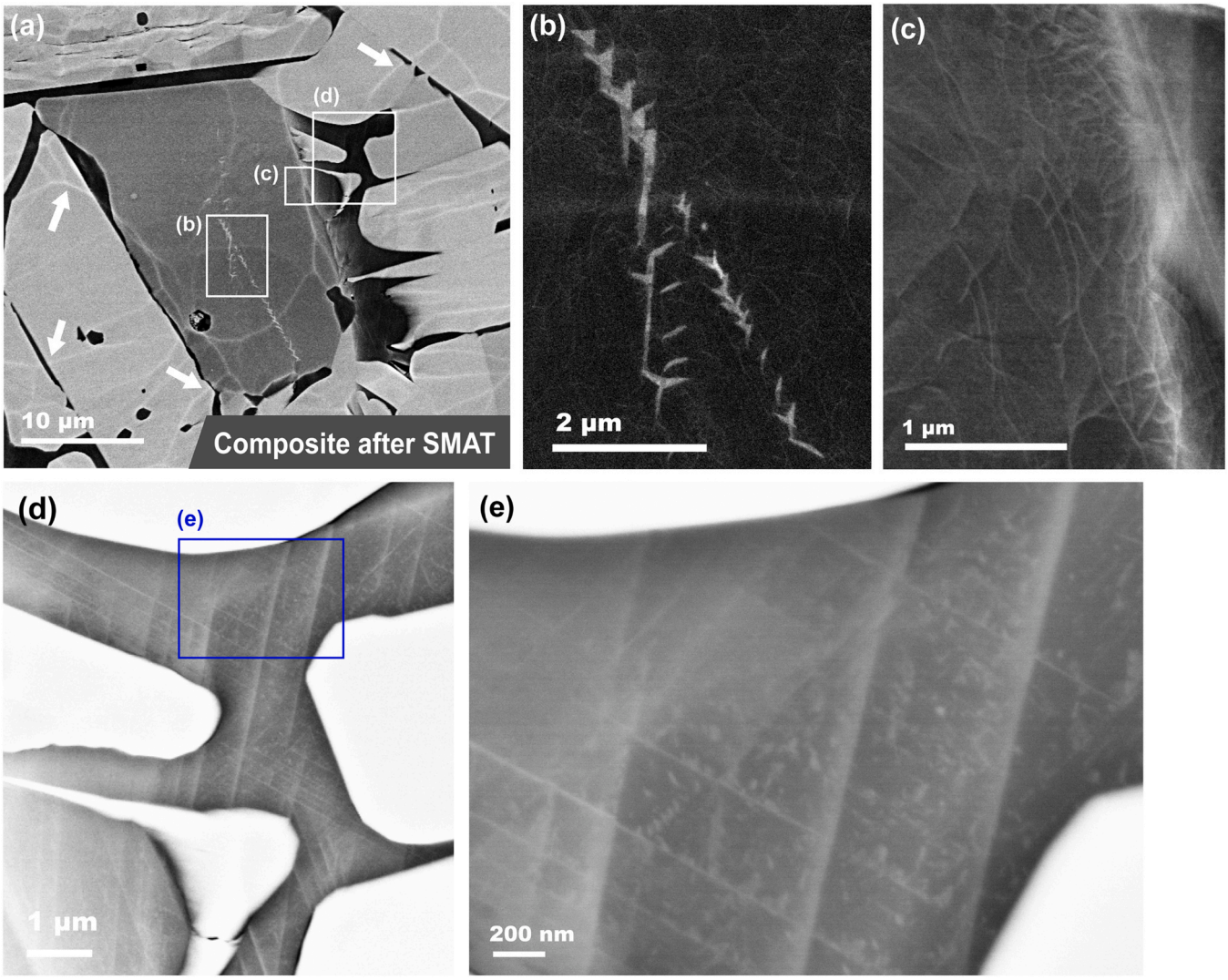

Fig. 6. BSE micrographs of the *composite material* in ECCI conditions. (b) dislocation wall within Ti_3AlC_2 (c) and dislocation networks near the grain boundary. (d,e) Parallel straight-lined defects in $TiAl_2$.

a microstructure gradient having nanoscale and/or submicrometric grain sizes extending over several tens of microns near the surface (Hall-Petch effect) and a deformed zone underneath [11,12,14,17]. During plastic deformation, mobile dislocations stored in the crystal gather into dislocation walls or low-angle grain boundaries (LAGBs). In highly deformed metals, the continuous increase in misorientation often leads to the progressive subdivision of grains in a continuous dynamic recrystallisation (CDRX) process [34]. For MAX phases, the formation of LAGBs leads to the formation of KBs, the main deformation mechanism of MAX phases. Such deformation mechanism has already been observed after SMAT by EBSD on a β-Ti alloy [35]. At further deformation, KBs cause delamination instead of CDRX and, in the absence of a binding cohesive phase, to a decohesion between the deformed MAX phase grains. Therefore, in our study the hardening after SMAT relies on different mechanisms than in the case of usually treated metals. Second, the extent of hardening is here limited to about 60% of the initial core material while it can reach values of hundreds of % in metals treated by SSPD and undergoing grain size refinement [12,14]. The increase of 60% in surface hardness is consistent with the degree of microstructure modification imparted by the SMAT to the *composite material* where both phases sustained the plastic deformation without grain refinement. The misorientation in Fig. 5 indicates that the MAX phase present within the *bulk material* was more highly strained than in the *composite material*, because of the absence of the binding Ti_2AlC phase having a damping effect. Thus, the damaging process of the MAX phase was more advanced in the bulk material, leading to delamination and decohesion.

For the *composite material*, the SEM analysis under ECCI conditions given in Fig. 6 has revealed structural defects in both the Ti_3AlC_2 MAX phase and the $TiAl_2$ intermetallic phase. The $TiAl_2$ phase surrounding the MAX phase blocks acts as a damping media providing with the ability to accumulate defects through the microstructure without triggering grain delamination and decohesion. This is the key parameter controlling the hardening of the *composite material* without losing structural integrity. This capacity was acquired due to the presence of the intergranular $TiAl_2$ which binds the MAX phase block system, thus preventing grain delamination and decohesion.

These results point to a promising new way to get around the brittleness of MAX phases, thus enabling SSPD for the surface hardening. To our knowledge, this is the first report on such a composite approach for MAX phases, although hardening via solid solution has recently been performed [36,37]. New phases are regularly added to the MAX compound family. Recent research successfully designed MABs compounds, with bore replacing

conventional X elements [38,39], or high entropy MAX phases [40,41]. As no additional element other than those composing the MAX phase are required to form the intermetallic phase, the composite approach can be easily implemented. The composite approach opens the way to the exploration of several combinations of intermetallics and MAX phases to adjust the resulting composite structure to the required mechanical properties.

5. Conclusion

In this study, a *bulk* Ti_2AlC MAX phase and a $Ti_3AlC_2/TiAl_2$ *composite* were deformed under SSPD by SMAT to test the effectiveness of a composite approach to strengthen the Ti-Al-C MAX phase system. The main conclusions can be listed as follows:

For the *bulk* MAX phase compound,

- SMAT applied on a *bulk* MAX phase damaged the surface and grain delamination followed by grain decohesion occurred.
- These damages were witnessed by a drop in surface hardness to a depth of 100 µm.
- Grain decohesion inhibits load transfer, so that no subsurface hardening was observed.

For the $MAX/TiAl_2$ *composite*,

- The binding $TiAl_2$ intergranular phase strengthens the MAX phase block system so that the cohesive *composite material* kept its structural integrity.
- Witness marks of deformation were observed in both MAX and $TiAl_2$ phases. Thus, the plasticity of both phases contributes to the hardening of the *composite material*.
- A load transfer was possible so that hardening of the *composite material* occurred to a depth of 250 µm with increased surface hardness of about 60%.

CRediT authorship contribution statement

Adrien Heinzelmeier: Conceptualization, Data curation, Investigation, Methodology, Writing – original draft, Writing – review & editing. Antoine Guitton: Conceptualization, Investigation, Methodology, Project administration, Supervision, Writing – original draft, Writing – review & editing. **Marc Novelli:** Conceptualization, Data curation, Investigation, Methodology, Writing – review & editing. **Wenbo Yu:** Resources, Writing – review & editing. **Thierry Grosdidier:** Conceptualization, Investigation, Methodology, Project administration, Supervision, Writing – review & editing

Data Availability

Data will be made available on request.

Declaration of Competing Interest

The authors declare that they have no known competing financial interests or personal relationships that could have appeared to influence the work reported in this paper.

Acknowledgment

This project has received financial supports from the CNRS through the MITI interdisciplinary programs.

The authors thank Olivier Perroud from LEM3, for his work on the XRD analysis presented in this paper.

References

[1] M.W. Barsoum, T. El-Raghy, The max phases: Unique new carbide and nitride materials, Am. Sci. 89 (2001) 334–343.
[2] M.W. Barsoum, M. Radovic, Elastic and mechanical properties of the MAX phases, Annu. Rev. Mater. Res. 41 (2011) 195–227, https://doi.org/10.1146/annurev-matsci-062910-100448
[3] M.W. Barsoum, T. El-Raghy, Synthesis and characterization of a remarkable ceramic: Ti3SiC2, J. Am. Ceram. Soc. 79 (1996) 1953–1956.
[4] A. Guitton, S. van Petegem, C. Tromas, A. Joulain, H. van Swygenhoven, L. Thilly, Effect of microstructure anisotropy on the deformation of MAX polycrystals studied by in-situ compression combined with neutron diffraction, Appl. Phys. Lett. 104 (2014), https://doi.org/10.1063/1.4884601
[5] N.G. Jones, C. Humphrey, L.D. Connor, O. Wilhelmsson, L. Hultman, H.J. Stone, F. Giuliani, W.J. Clegg, On the relevance of kinking to reversible hysteresis in MAX phases, Acta Mater. 69 (2014) 149–161, https://doi.org/10.1016/j.actamat.2014.01.045
[6] M.W. Barsoum, L. Farber, T. El-Raghy, Dislocations, Kink Bands, and Room-Temperature Plasticity of Ti 3 SiC 2, (1999) 1727–1738.
[7] G.P. Bei, A. Guitton, A. Joulain, V. Brunet, S. Dubois, L. Thilly, C. Tromas, Pressure-enforced plasticity in MAX phases: From single grain to polycrystal investigation, Philos. Mag. 93 (2013) 1784–1801, https://doi.org/10.1080/14786435.2012.755272
[8] Z. Zhan, M. Radovic, A. Srivastava, On the non-classical crystallographic slip in Tin+1AlCn MAX phases, Scr. Mater. 194 (2021), https://doi.org/10.1016/j.scriptamat.2020.113698
[9] A. Guitton, A. Joulain, L. Thilly, C. Tromas, Evidence of dislocation cross-slip in MAX phase deformed at high temperature, Sci. Rep. 4 (2014), https://doi.org/10.1038/srep06358
[10] E. Drouelle, A. Joulain, J. Cormier, V. Gauthier-Brunet, P. Villechaise, S. Dubois, P. Sallot, Deformation mechanisms during high temperature tensile creep of Ti3AlC2MAX phase, J. Alloy. Compd. 693 (2017) 622–630, https://doi.org/10.1016/j.jallcom.2016.09.194
[11] K. Lu, J. Lu, Nanostructured surface layer on metallic materials induced by surface mechanical attrition treatment, Mater. Sci. Eng. A 375–377 (2004) 38–45, https://doi.org/10.1016/j.msea.2003.10.261
[12] J. Azadmanjiri, C.C. Berndt, A. Kapoor, C. Wen, Development of surface nanocrystallization in alloys by surface mechanical attrition treatment (SMAT), Crit. Rev. Solid State Mater. Sci. 40 (2015) 164–181, https://doi.org/10.1080/10408436.2014.978446
[13] A. Heydari Astaraee, R. Miresmaeili, S. Bagherifard, M. Guagliano, M. Aliofkhazraei, Incorporating the principles of shot peening for a better understanding of surface mechanical attrition treatment (SMAT) by simulations and experiments, Mater. Des. 116 (2017) 365–373, https://doi.org/10.1016/j.matdes.2016.12.045
[14] T. Grosdidier, M. Novelli, Recent developments in the application of surface mechanical attrition treatments for improved gradient structures: Processing parameters and surface reactivity, Mater. Trans. 60 (2019) 1344–1355, https://doi.org/10.2320/matertrans.MF201929
[15] T.O. Olugbade, J. Lu, Literature review on the mechanical properties of materials after surface mechanical attrition treatment (SMAT), Nano Mater. Sci. 2 (2020) 3–31, https://doi.org/10.1016/j.nanoms.2020.04.002
[16] M. Novelli, J.J. Fundenberger, P. Bocher, T. Grosdidier, On the effectiveness of surface severe plastic deformation by shot peening at cryogenic temperature, Appl. Surf. Sci. 389 (2016) 1169–1174, https://doi.org/10.1016/j.apsusc.2016.08.009
[17] Y. Samih, B. Beausir, B. Bolle, T. Grosdidier, In-depth quantitative analysis of the microstructures produced by Surface Mechanical Attrition Treatment (SMAT), Mater. Charact. 83 (2013) 129–138, https://doi.org/10.1016/j.matchar.2013.06.006
[18] O. Unal, R. Varol, Surface severe plastic deformation of AISI 304 via conventional shot peening, severe shot peening and repeening, Appl. Surf. Sci. 351 (2015) 289–295, https://doi.org/10.1016/j.apsusc.2015.05.093
[19] M.W. Barsoum, M. Radovic, Elastic and mechanical properties of the MAX phases, Annu. Rev. Mater. Res. 41 (2011) 195–227, https://doi.org/10.1146/annurev-matsci-062910-100448
[20] W. Yu, M. Vallet, B. Levraut, V. Gauthier-Brunet, S. Dubois, Oxidation mechanisms in bulk Ti2AlC: Influence of the grain size, J. Eur. Ceram. Soc. 40 (2020) 1820–1828, https://doi.org/10.1016/j.jeurceramsoc.2020.01.042
[21] T. Nakano, A. Negishi, K. Hayashi, Y. Umakoshi, Ordering process of Al5Ti3, h-Al2Ti and r-Al2Ti with F.C.C.-based long-period superstructures in rapidly solidified Al-rich TiAl alloys., n.d.
[22] G.P. Bei, V. Gauthier-Brunet, C. Tromas, S. Dubois, Synthesis, characterization, and intrinsic hardness of layered nanolaminate Ti 3 AlC 2 and Ti 3 Al 0.8 Sn 0.2C 2 solid solution, J. Am. Ceram. Soc. 95 (2012) 102–107, https://doi.org/10.1111/j.1551-2916.2011.04846.x
[23] J.C. Schuster, M. Palm, Reassessment of the binary aluminum-titanium phase diagram, J. Phase Equilibria Diffus. 27 (2006) 255–277, https://doi.org/10.1361/154770306×109809
[24] N. v Tzenov, M.W. Barsoum, Synthesis and characterization of Ti3AlC2, Am. Ceram. Soc. 83 (2000) 825–832.
[25] A.R. Rastkar, P. Parseh, N. Darvishnia, S.M.M. Hadavi, Microstructural evolution and hardness of TiAl 3 and TiAl 2 phases on Ti-45Al-2Nb-2Mn-1B by plasma pack aluminizing, Appl. Surf. Sci. 276 (2013) 112–119, https://doi.org/10.1016/j.apsusc.2013.03.043

[26] B. Beausir, J.-J. Fundenberger, Analysis tools for electron and X-ray diffraction, ATEX—software, Available Online: Www. Atex-Software. Eu (Accessed on 28 March 2022). (2017).
[27] P. Morin, M. Pitaval, E. Vicario, G. Fontaine, Scanning Electron Microscope Observation of Single Defects in Solid Crystalline Materials, 1979.
[28] P. Morin, M. Pitaval, D. Besnard, G. Fontaine, Electron–channelling imaging in scanning electron microscopy, Philos. Mag. A: Phys. Condens. Matter Struct. Defects Mech. Prop. 40 (1979) 511–524, https://doi.org/10.1080/01418617908234856
[29] H. Kriaa, A. Guitton, N. Maloufi, Modelling electron channeling contrast intensity of stacking fault and twin boundary using crystal thickness effect, Materials 14 (2021), https://doi.org/10.3390/ma14071696
[30] H. Kriaa, A. Guitton, N. Maloufi, Fundamental and experimental aspects of diffraction for characterizing dislocations by electron channeling contrast imaging in scanning electron microscope, Sci. Rep. 7 (2017), https://doi.org/10.1038/s41598-017-09756-3
[31] H. Kriaa, A. Guitton, N. Maloufi, Modeling dislocation contrasts obtained by accurate-electron channeling contrast imaging for characterizing deformation mechanisms in bulk materials, Materials 12 (2019), https://doi.org/10.3390/ma12101587
[32] A. Guitton, A. Joulain, L. Thilly, C. Tromas, Dislocation analysis of Ti 2AlN deformed at room temperature under confining pressure, Philos. Mag. 92 (2012) 4536–4546, https://doi.org/10.1080/14786435.2012.715250
[33] A.W. Thompson, J.F. Knott, Micromechanisms of brittle fracture, Metall. Trans. A 24 (1993) 523–534.
[34] F.J. Humphreys, M. Hatherly, Recrystallization and Related Annealing Phenomena, Elsevier, 2004.
[35] P. Maurel, L. Weiss, P. Bocher, T. Grosdidier, Effects of SMAT at cryogenic and room temperatures on the kink band and martensite formations with associated fatigue resistance in a β-metastable titanium alloy, Mater. Sci. Eng. A. 803 (2021) 140618, https://doi.org/10.1016/j.msea.2020.140618
[36] R. Pan, J. Zhu, Y. Liu, Synthesis, microstructure and properties of (Ti1−x, Mox) 2AlC phases, Mater. Sci. Technol. 34 (2018) 1064–1069, https://doi.org/10.1080/02670836.2017.1419614
[37] M.A. Ali, S.H. Naqib, Recently synthesized (Ti1-: X Mo x)2AlC (0 ≤ x ≤ 0.20) solid solutions: Deciphering the structural, electronic, mechanical and thermodynamic properties via ab initio simulations, RSC Adv. 10 (2020) 31535–31546, https://doi.org/10.1039/d0ra06435a
[38] T. Rackl, L. Eisenburger, R. Niklaus, D. Johrendt, Syntheses and physical properties of the MAX phase boride Nb2SB and the solid solutions N b2 S Bx C1-x(x=0-1), Phys. Rev. Mater. 3 (2019), https://doi.org/10.1103/PhysRevMaterials.3.054001
[39] M.A. Ali, M.M. Hossain, M.M. Uddin, M.A. Hossain, A.K.M.A. Islam, S.H. Naqib, Physical properties of new MAX phase borides M2SB (M = Zr, Hf and Nb) in comparison with conventional MAX phase carbides M2SC (M = Zr, Hf and Nb): comprehensive insights, J. Mater. Res. Technol. 11 (2021) 1000–1018, https://doi.org/10.1016/j.jmrt.2021.01.068
[40] W. Bao, X.G. Wang, H. Ding, P. Lu, C. Zhu, G.J. Zhang, F. Xu, High-entropy M2AlC-MC (M=Ti, Zr, Hf, Nb, Ta) composite: synthesis and microstructures, Scr. Mater. 183 (2020) 33–38, https://doi.org/10.1016/j.scriptamat.2020.03.015
[41] S. Zhao, L. Chen, H. Xiao, J. Huang, Y. Li, Y. Qian, T. Zheng, Y. Li, L. Cao, H. Zhang, H. Liu, Y. Wang, Q. Huang, C. Wang, Phase transformation and amorphization resistance in high-entropy MAX phase M2SnC (M = Ti, V, Nb, Zr, Hf) under in-situ ion irradiation, Acta Mater. 238 (2022), https://doi.org/10.1016/j.actamat.2022.118222